

Chapter 10: Analysis of Temperature Derivatives (Sec. 10.3-10.4) *

Anatoliy Swishchuk

University of Calgary

'Lunch at the Lab' Talk

March 18th, 2010

*Book Review: 'Stochastic Modeling of Electricity and Related Markets'
by F. Benth, J. Benth & S. Koekebakker, 2008, World Sci. Publ.

Outline of Presentation

1. Empirical Analysis of Stockholm Temperature Dynamics (sec. 10.3)
2. Temperature Derivatives Pricing (sec. 10.4)

Empirical Analysis of Stockholm Temperature Dynamics (Sec. 10.3)

In this Section they study empirically the time series of *daily average temperature* (DATs) observed in Stockholm, Sweden, and fit an AR(p) model to these data.

Description of the Data (10.3.1.)

They have available DATs measured in degrees of Celcius from Stockholm over a period ranging from 1 January 1961 to 25 May 2006, resulting in 16,581 records. The DAT is calculated as the average of the minimum and maximum temperature during the day.

Empirical Analysis of Stockholm Temperature Dynamics (Sec. 10.3): Description of the Data (10.3.1.)

The measurement on February 29 was removed from the sample in each leap year to equalise the length of all years, leading to the time series of 16,570 observations.

DAT time series is plotted in Fig. 10.1 together with the fitted seasonal average described below. For illustrative purposes we only picture a snapshot of DAT's from the last 10 years of the data set.

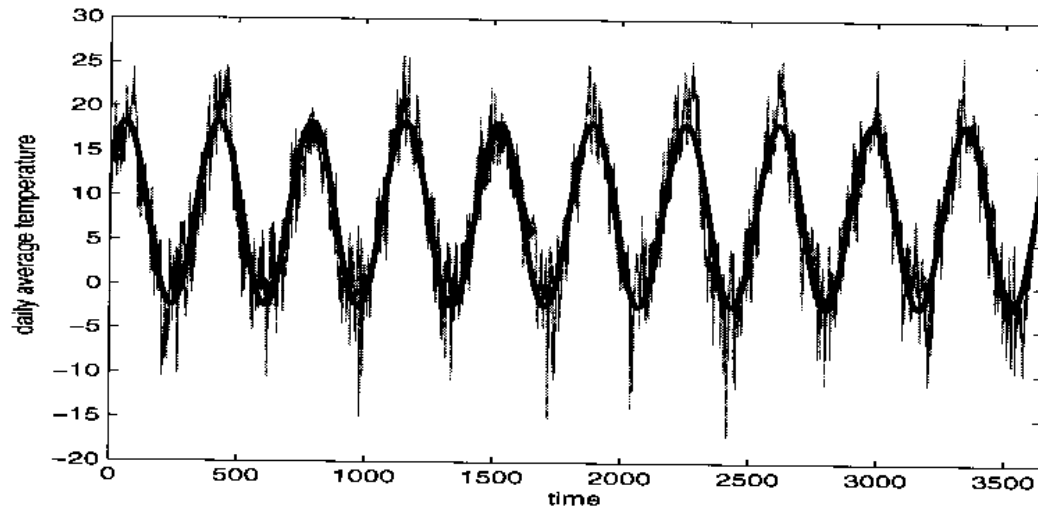


Fig. 10.1 DATs in Stockholm together with the fitted seasonal function, a snapshot of the last 10 years starting 25 May 1996.

Fig. 1. DAT Time Series

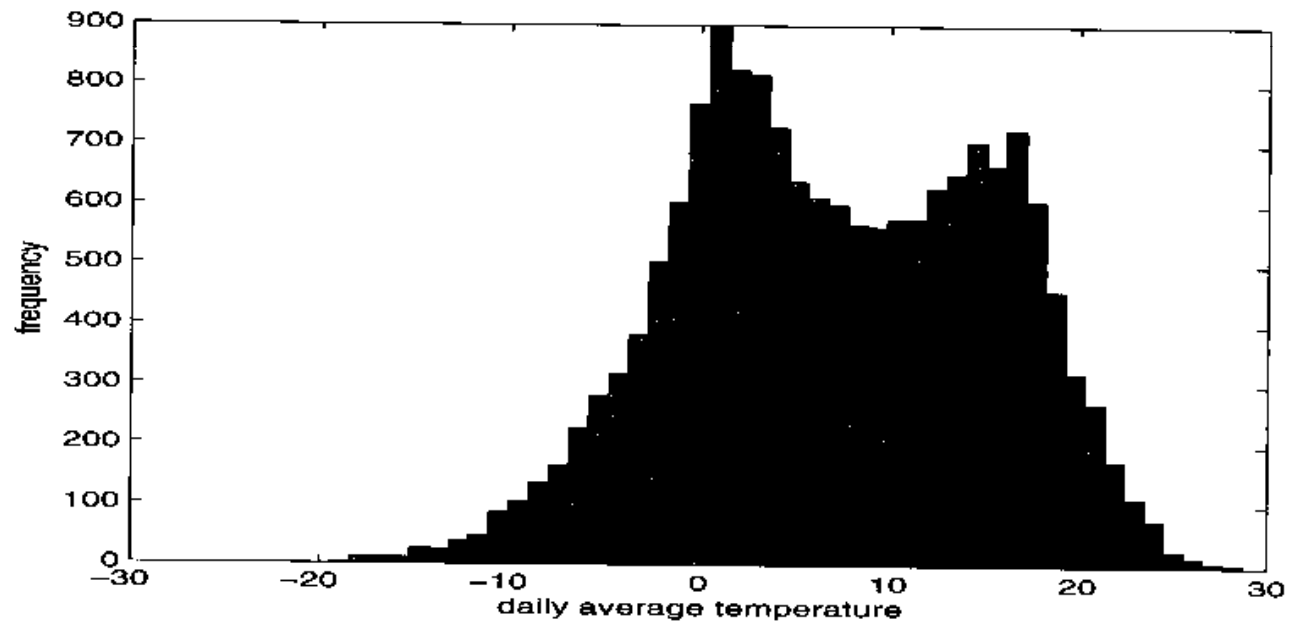


Fig. 10.2 Histogram of DATs in Stockholm.

Fig. 2. Non-normality of Data: Stockholm has cold winters and mild summer, which is reflected in a binomial histogram. Graph skewed to the left and has a negative kurtosis.

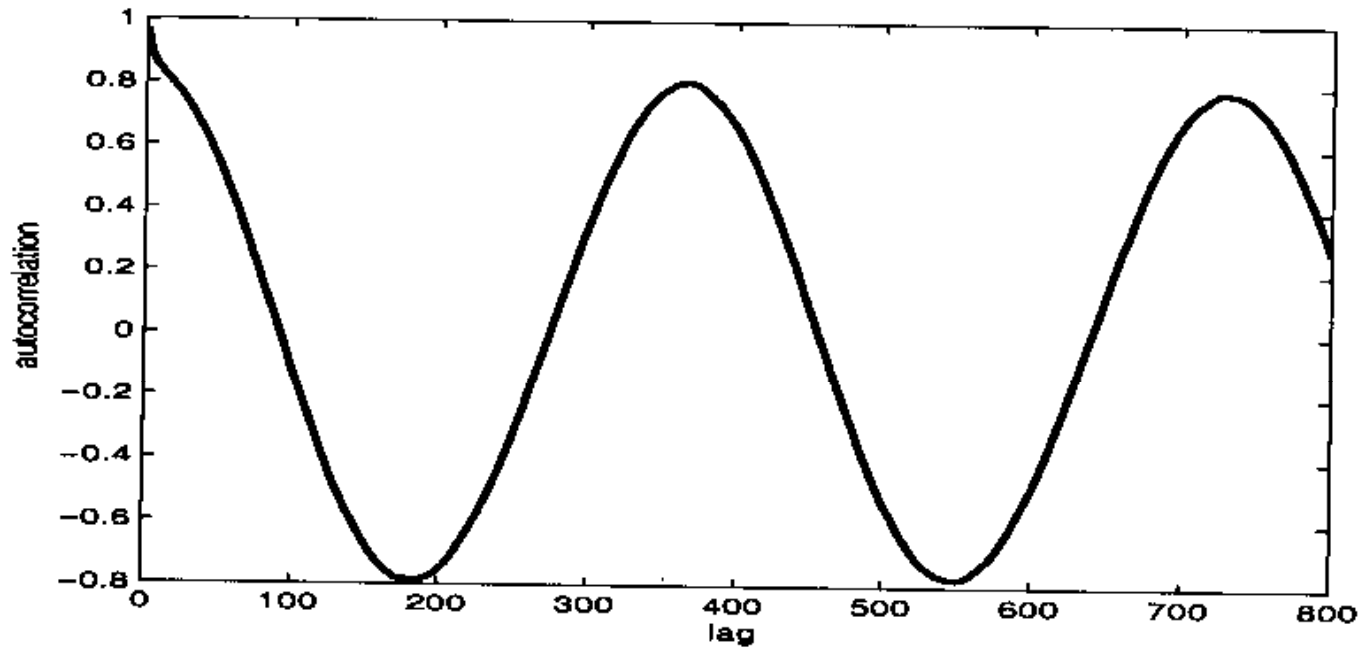


Fig. 10.3 Empirical ACF of DATs in Stockholm.

Fig. 3. We observe a strong seasonal variation.

Empirical Analysis of Stockholm Temperature Dynamics (Sec. 10.3): Estimating the CAR(p) Models (10.3.2.)

Suppose that the temperature on day $i = 0, 1, 2, \dots$ is denoted by T_i , and let

$$T_i = \Lambda_i + y_i, \quad \Lambda_i = \Lambda(i).$$

The function $\Lambda(t)$ is defined by

$$\Lambda(t) = a_0 + a_1 t + a_2 \cos(2\pi(t - a_3)/365),$$

where a_0 -average level of the t^o series, a_1 -slope of a linear trend function, a_2 -amplitude of the mean t^o , a_3 -phase angle. Time measured in days.

Empirical Analysis of Stockholm Temperature Dynamics (Sec. 10.3): Estimating the CAR(p) Models (10.3.2.)

t^o has a tendency to revert back to its mean over time. This mean-reverting property can be modelled by an AR(p) process and the choice $p = 3$ is the most suitable. We suppose that the deseasonalized t^o data $T(t) - \Lambda(t)$ can be modelled by AR(p) process y_i , with seasonal varying residuals

$$y_{i+p} = \sum_{j=1}^p b_j y_{i+p-j} + \sigma_i \epsilon_i, \quad \epsilon_i \sim N(0, 1), \quad i.i.d.r.v.$$

Empirical analysis suggests the following seasonal form of the volatility function

$$\sigma^2(t) = c_1 + \sum_{k=1}^4 (c_{2k} \cos(2k\pi t/365) + c_{2k+1} \sin(2k\pi t/365)).$$

Empirical Analysis of Stockholm Temperature Dynamics (Sec. 10.3): Estimating the CAR(p) Models (10.3.2.)

In the process of eliminating the parameters of the model, they eliminate step by step the different model component from the data:

- 1) detrend and deseasonalize the observed time series ($p = 1, 2$);
- 2) residuals obtained after eliminating the AR(p) process are not uncorrelated and far from being normal;
- 3) after the effect of estimated daily seasonal variance is removed from the data, the residuals become more much closer to normal and are slightly correlated. The choice of $p = 3$ gives a much better fit than $p = 1$. We now present the finding from the empirical analysis.

Empirical Analysis of Stockholm Temperature Dynamics (Sec. 10.3): Estimating the CAR(p) Models (10.3.2.)

The parameters are fitted using the method of least squares and estimates are reported in Table 10.1 below (The value of R^2 after estimating $\Lambda(t)$ is 80.9% showing a reasonable good fit):

Table 10.1

a_0	a_1	a_2	a_3
6.3759	0.0001	10.4411	– 165.7591

Empirical Analysis of Stockholm Temperature Dynamics (Sec. 10.3): Estimating the CAR(p) Models (10.3.2.)

They eliminate the linear trend and seasonal component by subtracting the estimated $\Lambda(t)$ from the original observations.

The ACF of the obtained residuals is plotted in Fig. 10.4

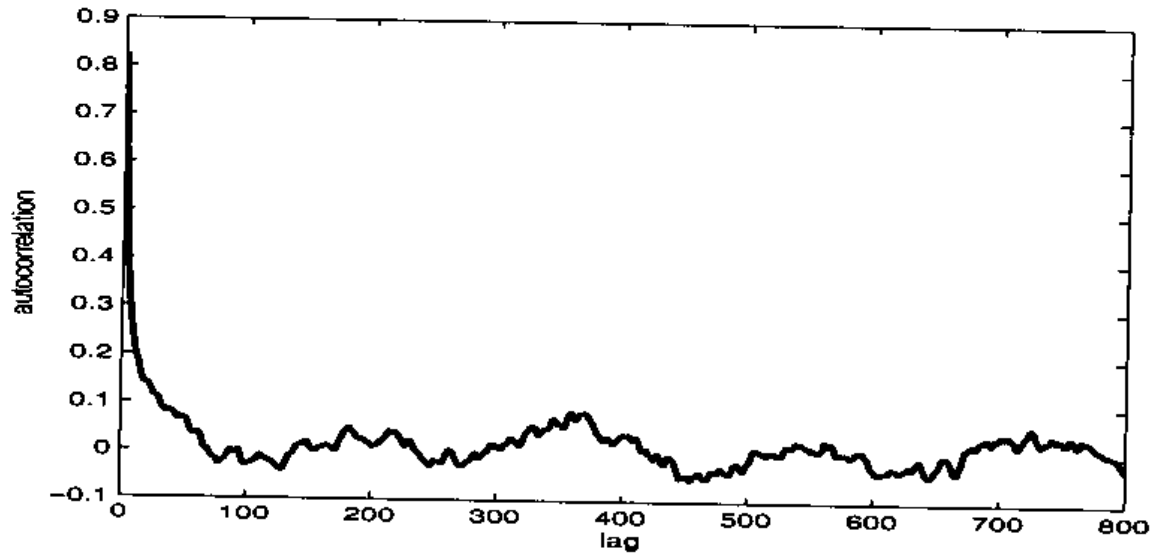


Fig. 10.4 The ACF of the residuals of DATs after linear trend and seasonal component were removed.

We see a pattern indicating an AR structure in the dynamics.

Empirical Analysis of Stockholm Temperature Dynamics (Sec. 10.3): Estimating the CAR(p) Models (10.3.2.)

The PACF plotted in Fig. 10.5 indicates that we need an $AR(3)$ process to explain the evolution in the time series data.

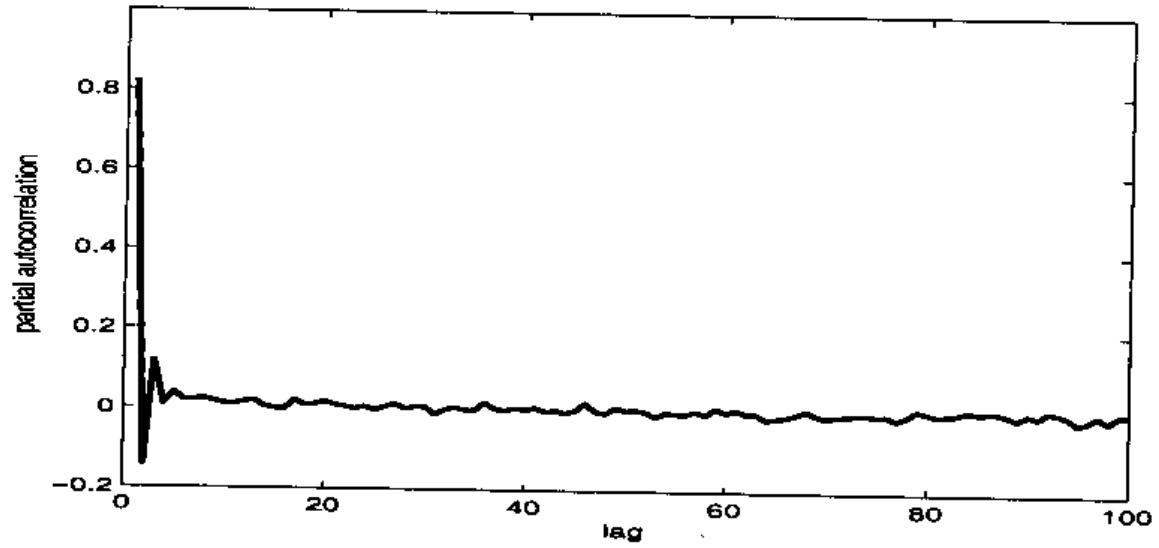


Fig. 10.5 The PACF of the residuals of DATs after linear trend and seasonal component were removed.

PACF plot

Empirical Analysis of Stockholm Temperature Dynamics (Sec. 10.3): Estimating the CAR(p) Models (10.3.2.): Fitting an AR(1) Model

An AR(1) may be a reasonable approx, and will correspond to an OU process.

Using an AR(3) model means that we base the t^o dynamics on the CAR(3) stochastic process. We fit both models here. They use a simple linear regression to estimate the parameter b_1 for the AR(1) process y_i defined above. By regressing today's detrended and deseasonalized t^o s against those of the previous day, they find $b_1 = 0.8234$, being significant at the 1% level.

The inclusion of the mean reversion process increased the value of R^2 to 93.9%. The histogram of the obtained residuals depicted in Fig. 10.6 seems to be close to normal.

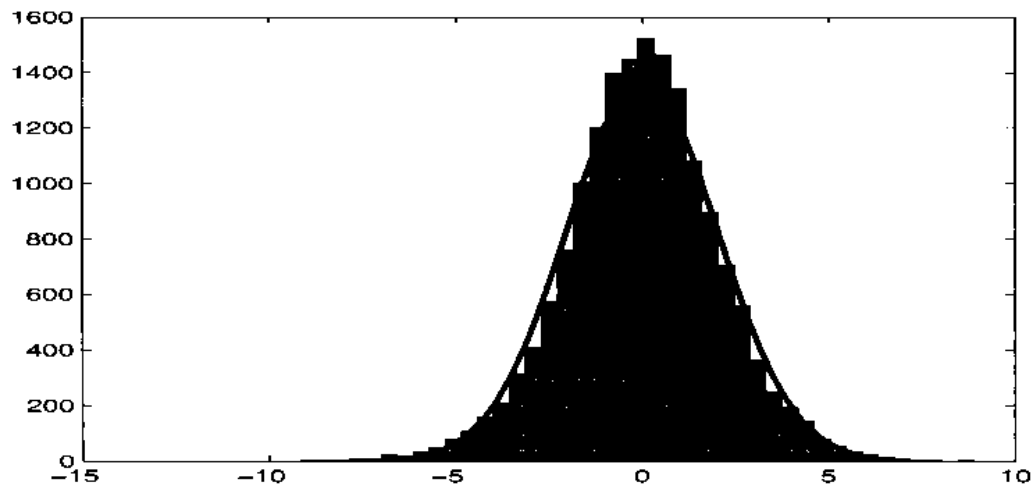


Fig. 10.6 Histogram of the residuals after linear trend, seasonal component and AR(1) process were removed.

Histogram of the residuals

Empirical Analysis of Stockholm Temperature Dynamics (Sec. 10.3): Estimating the CAR(p) Models (10.3.2.): Fitting an AR(1) Model

In Fig. 10.7 they plot the residuals and squared residuals for the last 10 years. We observe a clear persistent variation in the noise, which is a sign of seasonal heteroskedasticity.

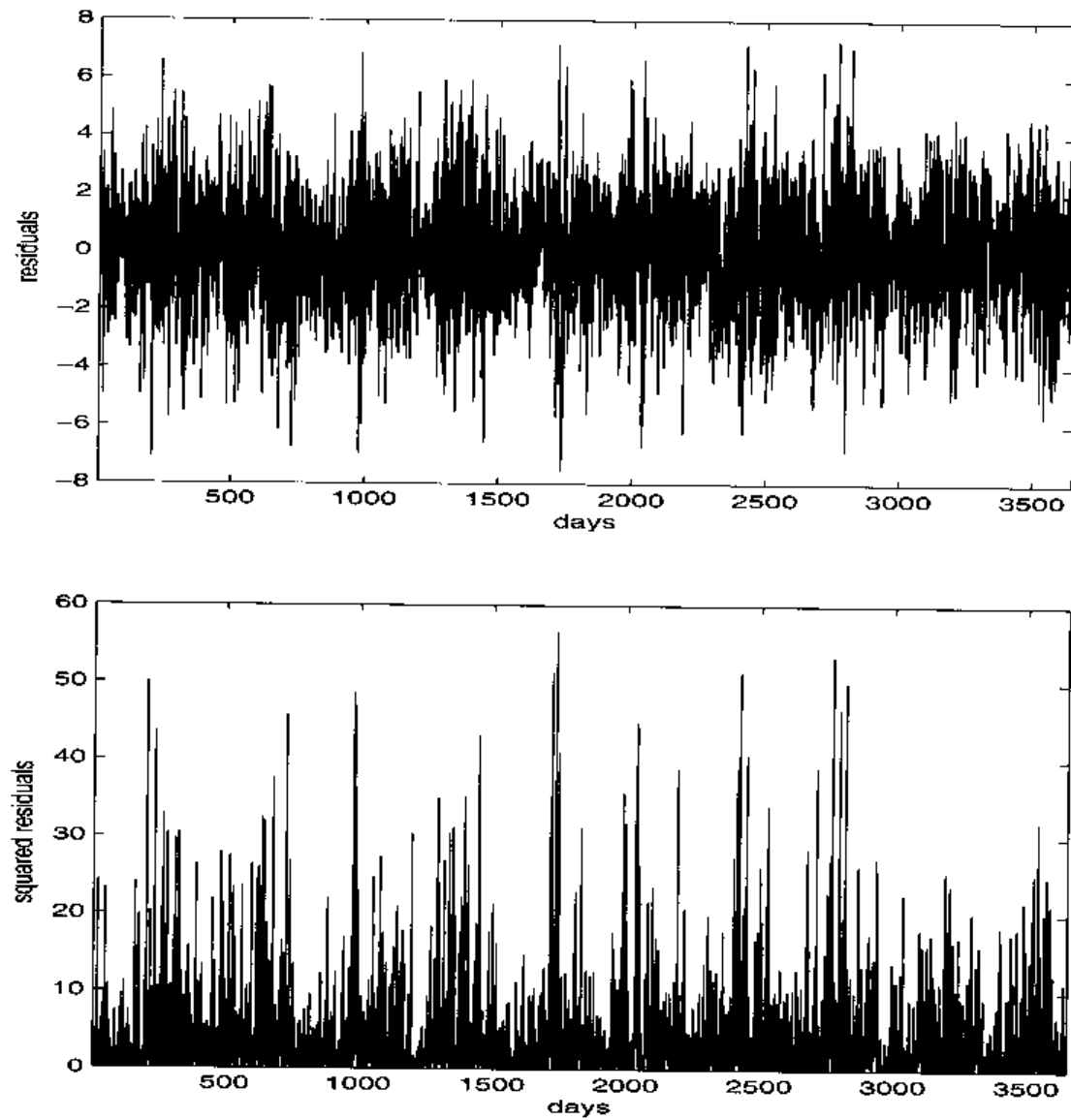


Fig. 10.7 Residuals and squared residuals of DATs after linear trend, seasonal component and AR(1) process were removed, a snapshot of the last 10 years starting 25 May 1996.

Empirical Analysis of Stockholm Temperature Dynamics (Sec. 10.3): Estimating the CAR(p) Models (10.3.2.): Fitting an AR(1) Model

This observation hints to the inclusion of a deterministic seasonality function when modelling the variance. Looking at the ACF for the residuals in Fig. 10.8 we see that ACs for the first two lags are quite high but decrease very rapidly and vary around zero for higher lags.

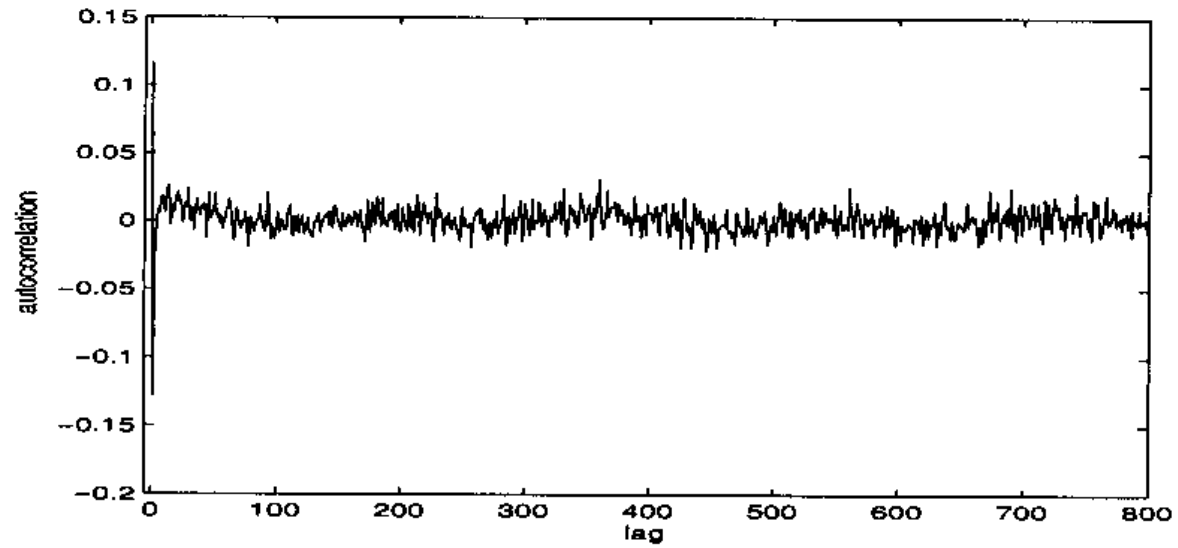


Fig. 10.8 ACF of residuals of DATs after linear trend, seasonal component and AR(1) process were removed.

ACF of residuals of DATs without trend, seasonal component and AR(1)

Empirical Analysis of Stockholm Temperature Dynamics (Sec. 10.3): Estimating the CAR(p) Models (10.3.2.): Fitting an AR(1) Model

The ACF of the squared residuals in Fig. 10.9 reveals a clear seasonal pattern in DAT for Stockholm, again pointing to a seasonal heteroskedasticity of the residuals.

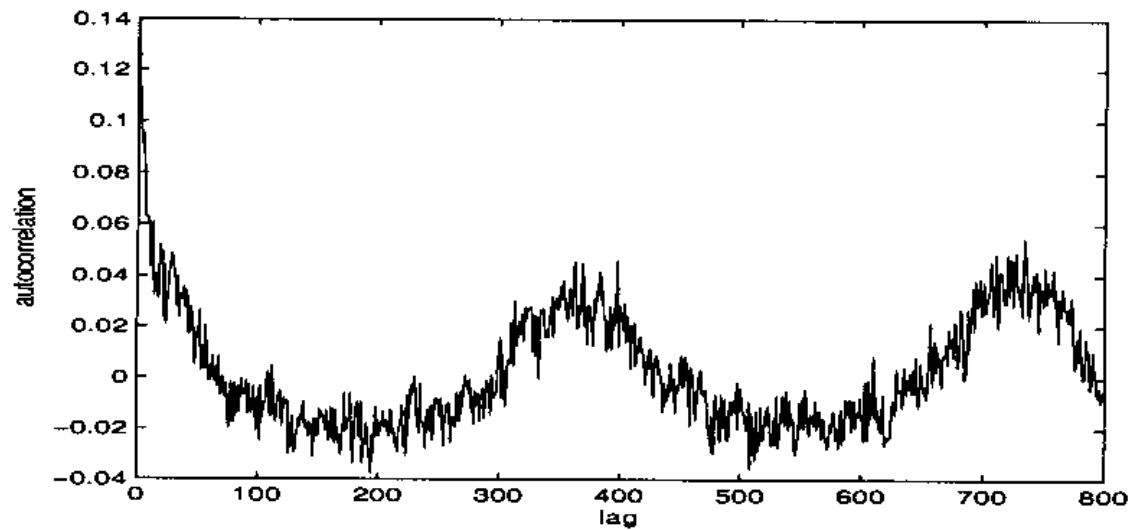


Fig. 10.9 ACF of squared residuals of DATs after linear trend, seasonal component and AR(1) process were removed.

ACF of squared residuals of DATs without trend, seasonal component and AR(1)

They continue with fitting the seasonal variance function $\sigma^2(t)$ defined before to the obtained residuals. The parameters are estimated using the least square approach. The fitted parameters are presented in Table 10.2.

Table 10.2 Fitted parameters of $\sigma^2(t)$ for the AR(1) case

c_1	c_2	c_3	c_4	c_5	c_6	c_7	c_8	c_9
4.151	1.358	0.702	0.807	-0.143	0.181	0.446	-0.054	-0.002

In Fig. 10.10 they present the empirical $\sigma^2(t)$ function together with the fitted one. It is obvious that the fluctuations in the cold season are considerably higher than those during the milder seasons. We see a clear seasonal volatility effect in the temperature data.

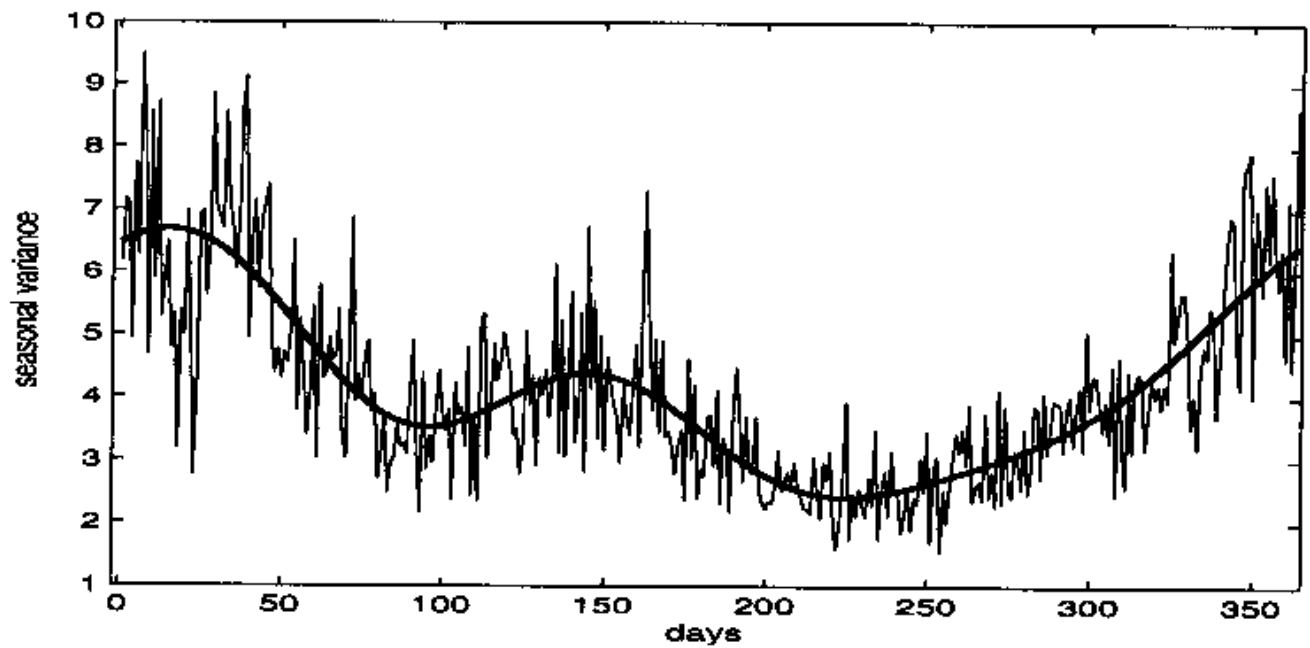


Fig. 10.10 Empirical and fitted $\sigma^2(t)$ function when AR(1) is used.

They eliminate the influence of the seasonal variation function from the data by dividing the residuals by the square root of the fitted $\sigma^2(t)$ function. The residuals histogram in Fig. 10.11 became closer to normal compared with the one in Fig. 10. 6.

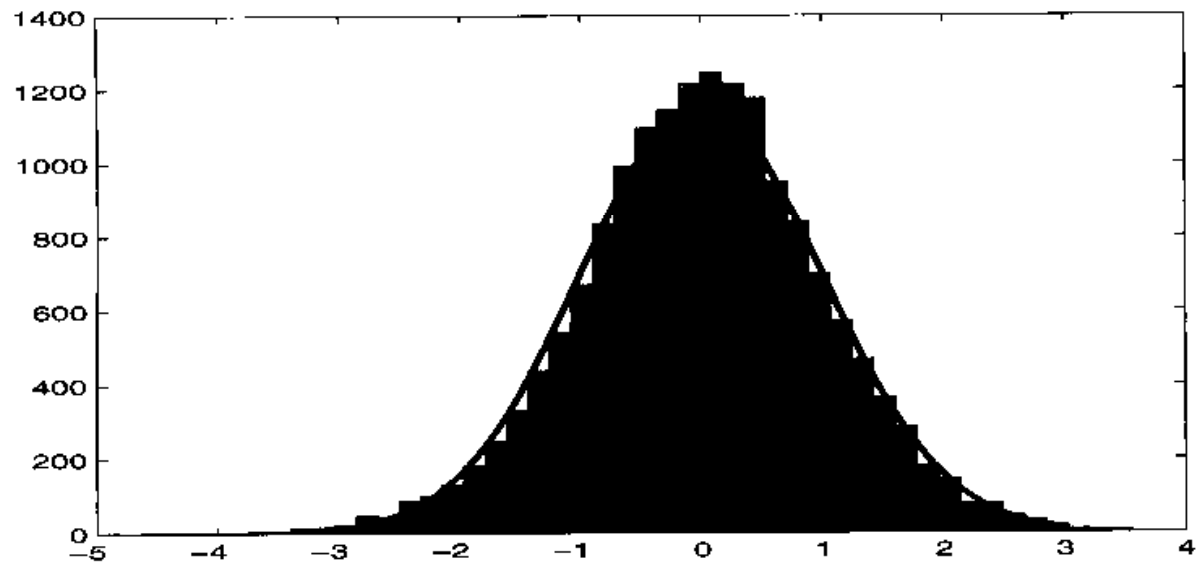


Fig. 10.11 Histogram of the residuals after linear trend, seasonal component, A process and seasonal variance were removed.

As we see from the normal plot Fig. 10.12, the reason for rejecting the normal distribution can be heavier tails than normal for negative residuals. An alternative approach based on the GH Lévy processes is suggested in Benth *et al.* (2005).

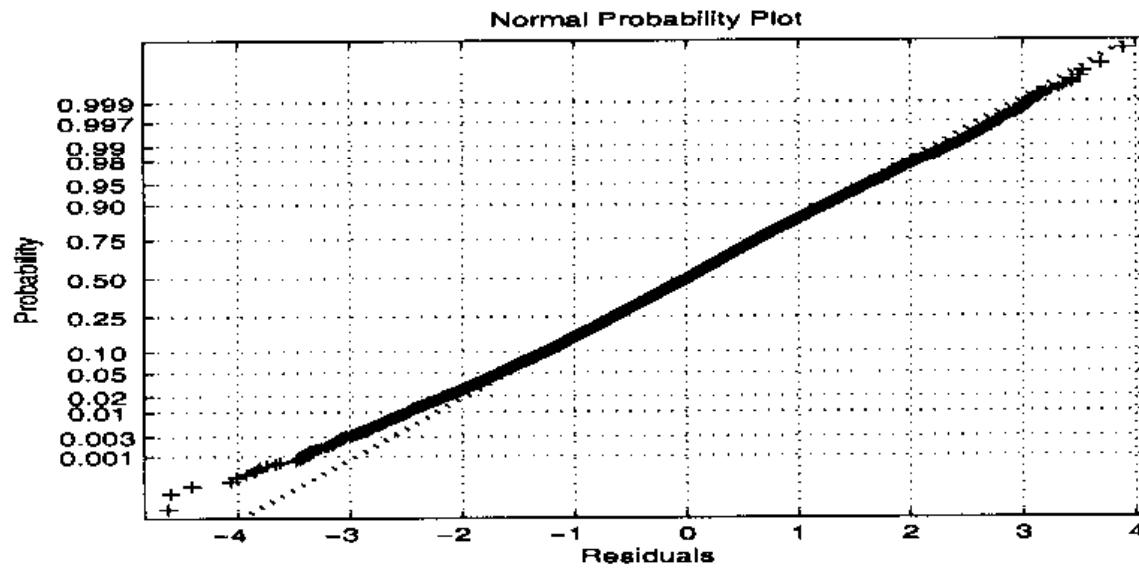


Fig. 10.12 Normal plot of the residuals after linear trend, seasonal component, AR(1) process and seasonal variance were removed.

The ACFs for residuals and squared residuals obtained after eliminating the seasonally dependent variance are plotted in Fig. 10.13 and Fig. 10.14, respectively.

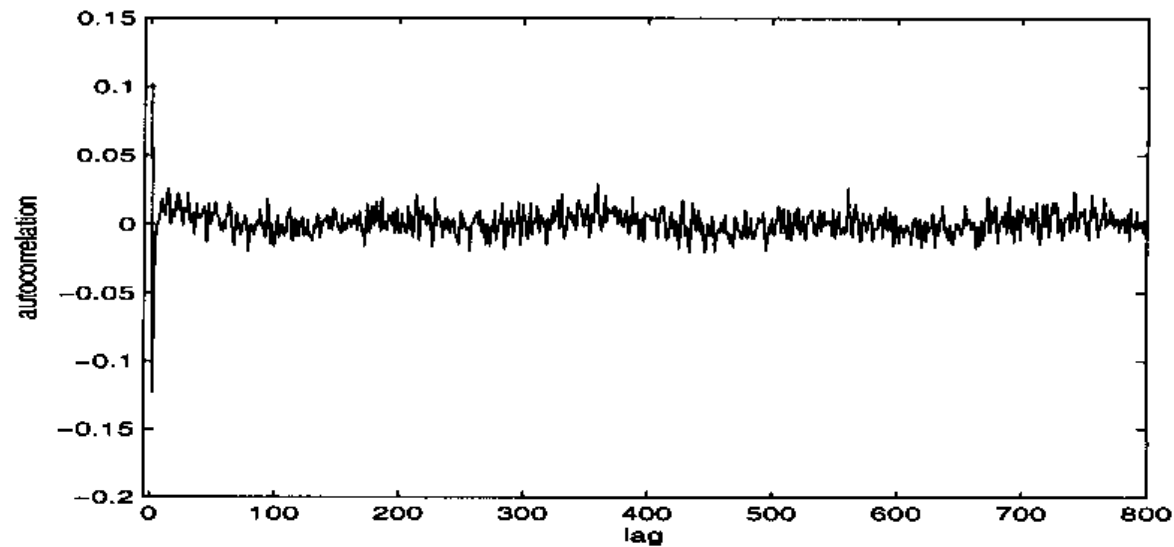


Fig. 10.13 ACF of residuals of DATs after linear trend, seasonal component, AR(1) process and seasonal variance were removed.

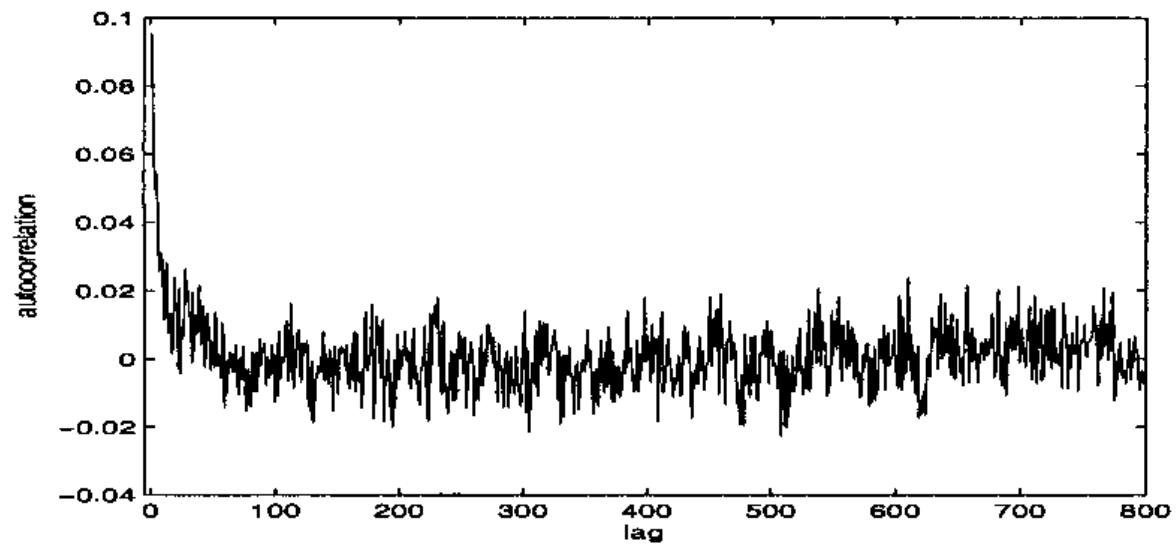


Fig. 10.14 ACF of squared residuals of DATs after linear trend, seasonal component, AR(1) process and seasonal variance were removed.

Empirical Analysis of Stockholm Temperature Dynamics (Sec. 10.3): Fitting an AR(3) Model (Sec. 10.3.2.2)

Motivated by the PACF in Fig. 10.5, they fit an AR(3) process to the detrended and deseasonalized data. The steps fitting the AR(3) model with seasonal variance follows the sequence above closely, and they report ony main results.

The values of the regression parameters are all significant at the 1% level and reported in Table 10.3. The model fit increased slightly compared to the AR(1) case, yielding $R^2 = 94.1\%$. The ACF of the residuals is presented in Fig. 10.15.

Table 10.3 Fitted regression parameters of the AR(3) process

b_1	b_2	b_3
0.957	-0.253	0.119

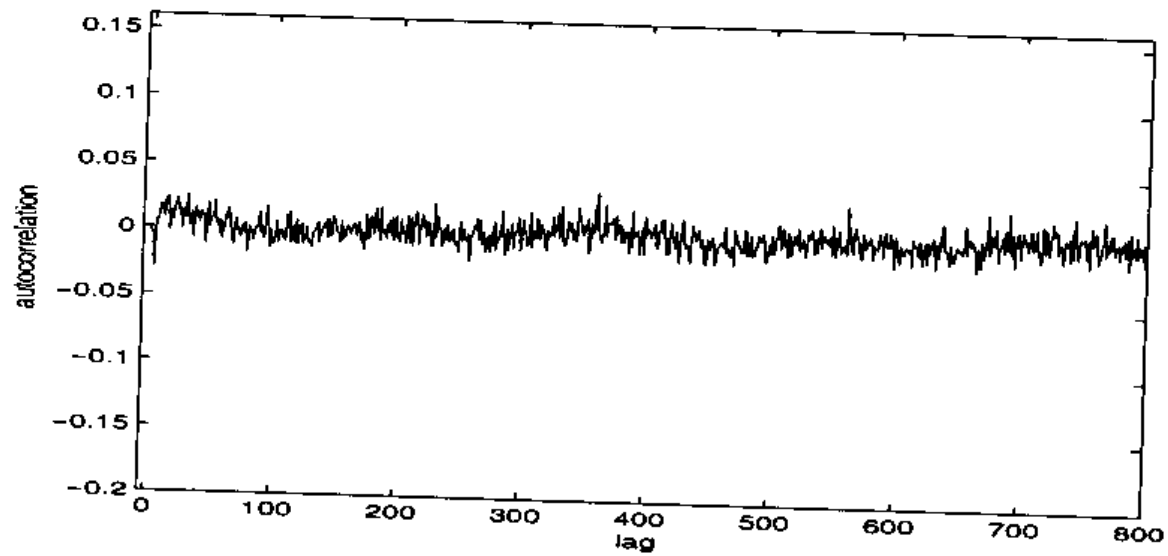


Fig. 10.15 ACF of residuals of DATs after linear trend, seasonal component and AR(3) process were removed.

As for the AR(1) model, we still have a distinct seasonality in the ACF for the squared residuals, as seen in Fig. 10.16.

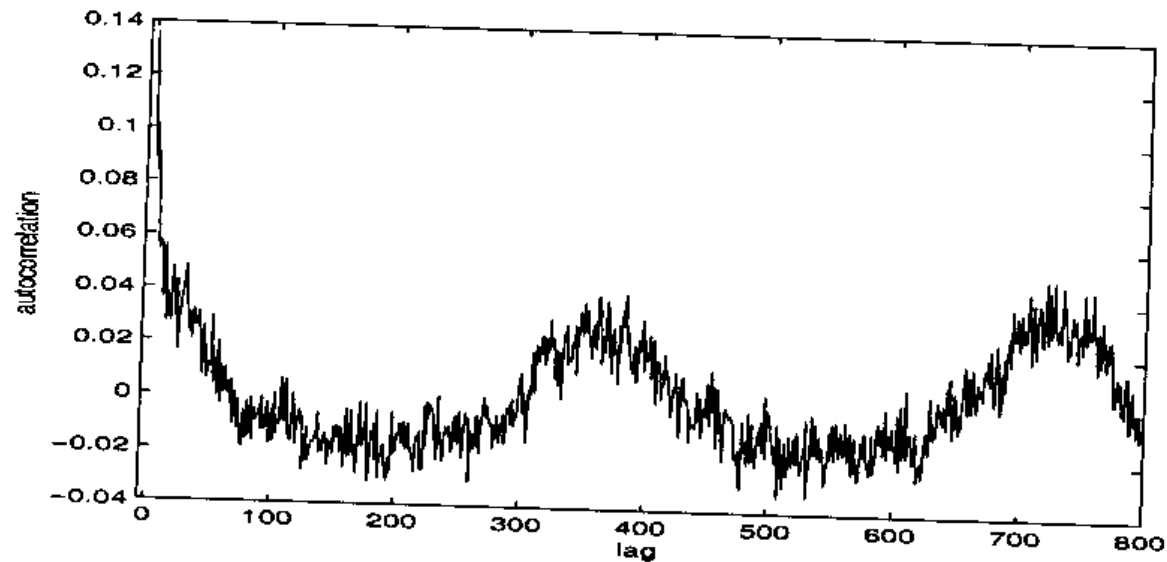


Fig. 10.16 ACF of squared residuals of DATs after linear trend, seasonal component and AR(3) process were removed.

The empirical and fitted seasonal variance functions are plotted in Fig. 10.17, and similar to the $AC(1)$ case. The estimated parameters are reported in Table 10.4. The estimates are quite close to those reported in Table 10.2.

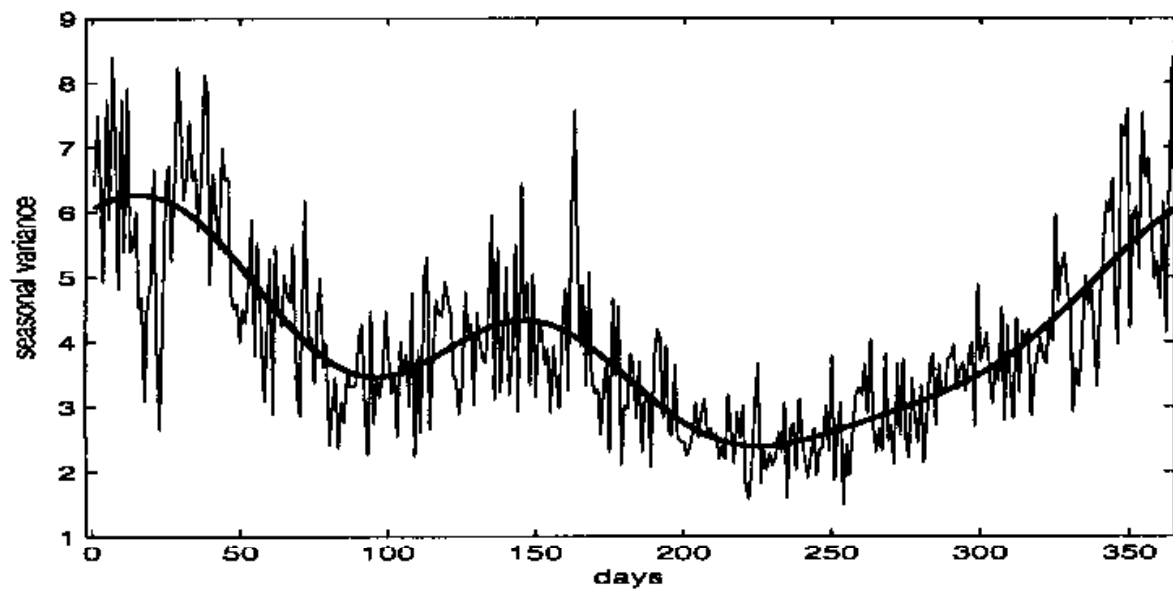


Fig. 10.17 Empirical and fitted $\sigma^2(t)$ function when AR(3) is used.

Table 10.4 Fitted parameters of $\sigma^2(t)$ for the AR(3) case

c_1	c_2	c_3	c_4	c_5	c_6	c_7	c_8	c_9
4.011	1.176	0.681	0.740	0.151	0.153	0.429	-0.042	-0.015

The ACFs for the obtained residuals are plotted in Fig. 10.18 and became smaller.

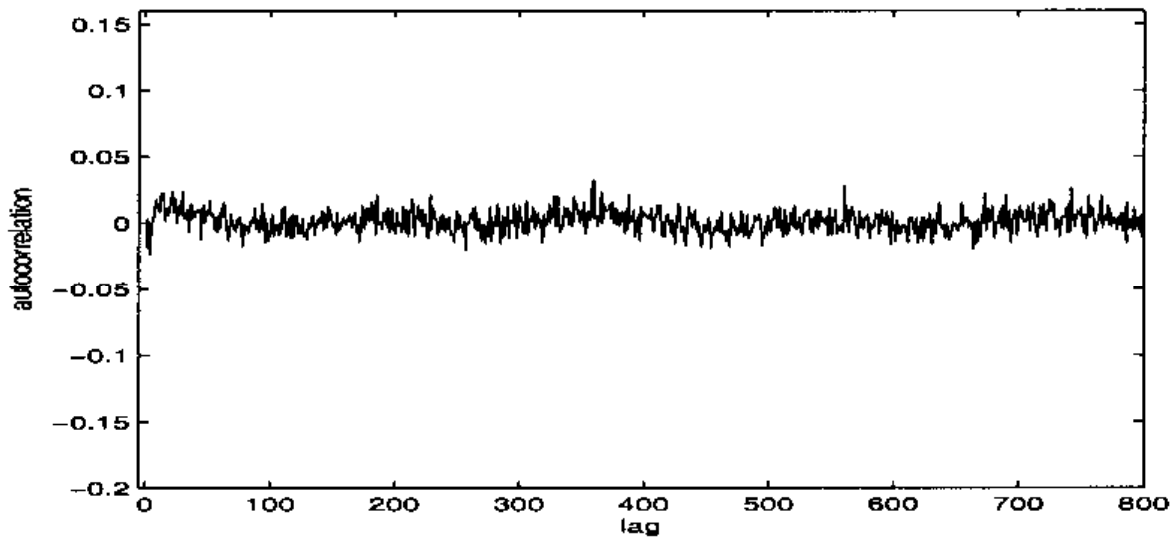


Fig. 10.18 ACF of residuals of DAT after linear trend, seasonal component, AR(3) process and seasonal variance were removed.

The ACF of squared residuals shown in Fig. 10.19 has the same structure as in the AR(1) case.

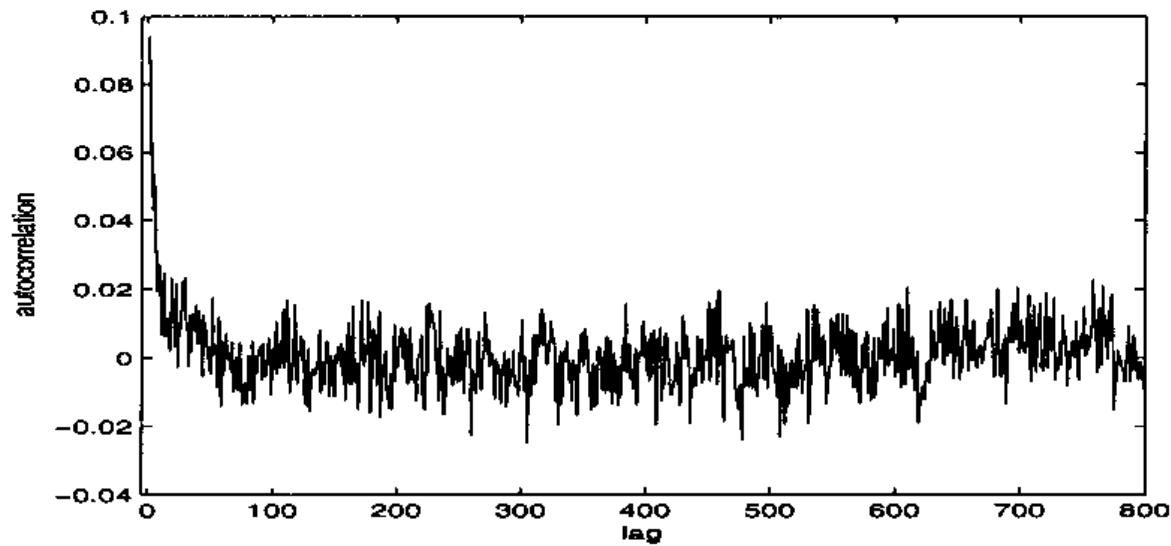


Fig. 10.19 ACF of squared residuals of DAT after linear trend, seasonal component, AR(3) process and seasonal variance were removed.

Empirical Analysis of Stockholm Temperature Dynamics (Sec. 10.3): Fitting an AR(3) Model (Sec. 10.3.2.2)

They conclude that the AR(3) process explains the data significantly better than the AR(1), and they give priority to this model.

Empirical Analysis of Stockholm Temperature Dynamics (Sec. 10.3): Identification of the parameters in the CAR(p) Model (Sec. 10.3.2.3)

The final step is to identify the corresponding parameters of the CAR(1) and CAR(3) models from the estimated parameters in the AC(1) and AC(3) models, respectively. The estimate of $b_1 = 0.8234$ and for $\alpha_1 = 0.1766$ (speed of mean-reversion in the CAR(1) dynamics).

As for the CAR(3) model, the all figures are reported in Table 10.5.

Table 10.5 Fitted regression parameters of the CAR(3) process

α_1	α_2	α_3
2.043	1.339	0.177

Temperature Derivatives Pricing (Sec. 10.4)

The temperature is modelled by a CAR(p) process and they concentrate on HDD, CDD and CAT futures, which constitute the three classes of futures products at CME. Along with the derivation of futures prices, they also discuss the valuation of European call and put options written on the futures. Finally, they analyse the Frost Day index futures.

Temperature Derivatives Pricing (Sec. 10.4): CAT Futures (Sec. 10.4.1)

The CAT futures price dynamics is defined by the risk-neutral conditional expectation

$$F_{CAT}(t, \tau_1, \tau_2) = E_Q\left[\int_{\tau_1}^{\tau_2} T(u)du \mid \mathcal{F}_t\right].$$

They restrict their attention the risk-neutral probabilities q^θ .

Prop. 10.2. The CAT futures price is given by

$$\begin{aligned} F_{CAT}(t, \tau_1, \tau_2) &= \int_{\tau_1}^{\tau_2} \Lambda(u)du + \mathbf{a}(t, \tau_1, \tau_2)\mathbf{X}(t) \\ &+ \int_{\tau_1}^{\tau_2} \theta(u)\sigma(u)\mathbf{a}(t, \tau_1, \tau_2)\mathbf{e}_p du \\ &+ \int_{\tau_1}^{\tau_2} \theta(u)\sigma(u)\mathbf{e}'_1 A^{-1}[\exp(A(\tau_2 - u)) - I_{p \times p}]\mathbf{e}_p du, \end{aligned}$$

where

$$\mathbf{a}(t, \tau_1, \tau_2) = \mathbf{e}'_1 A^{-1}[\exp(A(\tau_2 - u)) - \exp(A(\tau_1 - u))].$$

Temperature Derivatives Pricing (Sec. 10.4): CAT Futures (Sec. 10.4.1)

The dynamics of the CAT futures price under Q^θ is given in the following Prop.

Prop. 10.3. The Q^θ dynamics of $F_{CAT}(t, \tau_1, \tau_2)$ is

$$dF_{CAT}(t, \tau_1, \tau_2) = \sum_{CAT} (t, \tau_1, \tau_2) dB^\theta(t),$$

where

$$\sum_{CAT} (t, \tau_1, \tau_2) = \sigma(t) e_1' A^{-1} [\exp(A(\tau_2 - u)) - \exp(A(\tau_1 - u))] e_p.$$

Temperature Derivatives Pricing (Sec. 10.4): CAT Futures (Sec. 10.4.1)

Prop. 10.4. The price at time t of a call option written on a CAT futures with strike K at exercise time $\tau \leq \tau_1$ and measurement period $[\tau_1, \tau_2]$ is

$$C_{CAT}(t, \tau, \tau_1, \tau_2) = e^{-r(\tau-t)} [(F_{CAT}(t, \tau_1, \tau_2) - K)\Phi(d(t, \tau, \tau_1, \tau_2))] + \int_t^\tau \Sigma_{CAT}^2(s, \tau_1, \tau_2) ds \Phi'(d(t, \tau, \tau_1, \tau_2)),$$

where

$$d(t, \tau, \tau_1, \tau_2) = \frac{F_{CAT}(t, \tau_1, \tau_2) - K}{\sqrt{\int_t^\tau \Sigma_{CAT}^2(s, \tau_1, \tau_2) ds}},$$

and Φ is the cumulative standard normal distribution function.

Temperature Derivatives Pricing (Sec. 10.4): CAT Futures (Sec. 10.4.1)

Prop. 10.5. The delta of the call option (or the hedge ratio) is given by

$$\frac{\partial C_{CAT}(t, \tau, \tau_1, \tau_2)}{\partial F_{CAT}(t, \tau_1, \tau_2)} = \Phi(d(t, \tau, \tau_1, \tau_2)).$$

Temperature Derivatives Pricing (Sec. 10.4): HDD/CDD Futures (Sec. 10.4.2)

They derive the explicit CDD futures dynamics, and discuss issues on pricing of options. Recall the price of a CDD futures to be

$$F_{CDD}(t, \tau_1, \tau_2) = E_Q\left[\int_{\tau_1}^{\tau_2} \max(T(s) - c, 0) | \mathcal{F}_t\right].$$

Temperature Derivatives Pricing (Sec. 10.4): HDD/CDD Futures (Sec. 10.4.2)

Prop. 10.6 The CDD futures price is given by

$$F_{CDD}(t, \tau_1, \tau_2) = \int_{\tau_1}^{\tau_2} v(t, s) \Psi\left(\frac{m(t, s, \mathbf{e}'_1) \exp(A(s-t)) \mathbf{X}(t)}{v(t, s)}\right) ds,$$

where

$$m(t, s, x) = \Lambda(s) - c + \int_t^s \sigma(u) \theta(u) \mathbf{e}'_1 \exp(A(s-t)) \mathbf{e}_p du + x,$$

$$v^2(t, s) = \int_t^s \sigma^2(u) (\mathbf{e}'_1 \exp(A(s-t)) \mathbf{e}_p)^2 du$$

and $\Psi(x) = x\Phi(x) + \Phi'(x)$, with Φ being the cumulative standard normal distribution function.

Temperature Derivatives Pricing (Sec. 10.4): HDD/CDD Futures (Sec. 10.4.2)

The dynamics of the CDD futures price is stated in the next Prop.

Prop. 10. 7. The dynamics of $F_{CDD}(t, \tau_1, \tau_2)$ under Q^θ is given by

$$dF_{CDD}(t, \tau_1, \tau_2) = \sigma(t) \int_{\tau_1}^{\tau_2} e_1' \exp(A(s-t)) e_p \times \Phi\left(\frac{m(t,s,e_1') \exp(A(s-t)) \mathbf{X}(t)}{v(t,s)}\right) ds dB^\theta(t).$$

Temperature Derivatives Pricing (Sec. 10.4): HDD/CDD Futures (Sec. 10.4.2)

The following proposition states the price of a CDD futures option at time $t \leq \tau$.

Prop. 10. 8. The price at time $t \leq \tau$ of a call option written on a CDD futures with measurement period $[\tau_1, \tau_2]$ and strike price K at the exercise time τ is given as

$$C_{CDD}(t, \tau, \tau_1, \tau_2) = e^{-r(\tau-t)} \times E[\max(\int_{\tau_1}^{\tau_2} v(\tau, s)Z(t, \tau, s, x)ds - K, 0)]_{x=\mathbf{X}(t)},$$

Temperature Derivatives Pricing (Sec. 10.4): HDD/CDD Futures (Sec. 10.4.2)

with the random field Z defined as follows

$$Z = \tilde{\Psi}(\tau, s, \mathbf{e}'_1 \exp(A(s-t)))x + \int_t^\tau \mathbf{e}'_1 \exp(A(s-t)) \mathbf{e}_p \sigma(u) \theta(u) du + \Sigma(s, t, \tau)Y.$$

Here,

$$\Sigma = \int_t^\tau (\mathbf{e}'_1 \exp(A(s-t)) \mathbf{e}_p)^2 \sigma^2(u) du, \quad Y \sim N(0, 1).$$

Temperature Derivatives Pricing (Sec. 10.4): HDD/CDD Futures (Sec. 10.4.2)

The hedging strategy for a call option written on CDD futures involves Malliavin calculus, in particular, Malliavin derivative, and we skip Prop. 10.9 and Prop. 10.10 as we did not learn it at our seminar.

Temperature Derivatives Pricing (Sec. 10.4): Frost Day Index Futures (Sec. 10.4.3)

They discuss the pricing of the Amsterdam Frost Day index futures traded at the CME. Recall the Frost Day index futures price is

$$F_{FDI}(t, \tau_1, \tau_2) = E_Q \left[\sum_{s=\tau_1}^{\tau_2} FD(s) | \mathcal{F}_t \right].$$

We have that $T(s)$ conditioned on \mathcal{F}_t is normally distributed under Q^θ . The expectation and variance of $T(s)$ are

$$\begin{aligned} m_{s,t} &= E_\theta [T(s) | \mathcal{F}_t] = \Lambda(s) + \mathbf{e}'_1 \exp(A(s-t)) \mathbf{X}(t) \\ &\quad + \int_t^s \mathbf{e}'_1 \exp(A(s-u)) \mathbf{e}_p \sigma(u) \theta(u) du \end{aligned}$$

and

$$v_{s,t}^2 = \text{Var}_\theta [T(s) | \mathcal{F}_t] = \int_t^s (\mathbf{e}'_1 \exp(A(s-u)) \mathbf{e}_p)^2 \sigma^2(u) du.$$

Temperature Derivatives Pricing (Sec. 10.4): Frost Day Index Futures (Sec. 10.4.3)

Since the temperatures at 7am and 10am define the Frost Day index, we need correlation between these two temperatures:

$$\begin{aligned}\rho_{s,t} &= \text{Corr}[T(s + 7/24), T(s + 10/24)|\mathcal{F}_t] \\ &= \frac{1}{v_{s+7/24,t}v_{s+10/24,t}} \int_t^{s+7/24} e_1' \exp(A(s + 7/24 - u)) e_p \\ &\quad \times e_1' \exp(A(s + 10/24 - u)) e_p \sigma^2(u) du.\end{aligned}$$

Temperature Derivatives Pricing (Sec. 10.4): Frost Day Index Futures (Sec. 10.4.3)

Prop. 10.11. A Frost Day index futures price at time t with measurement period $[\tau_1, \tau_2]$ is given by

$$\begin{aligned}
 F_{FDI}(t, \tau_1, \tau_2) &= \sum_{s=\tau_1}^{\tau_2} \Phi\left(\frac{-3.5-m_s+7/24,t}{v_s+7/24,t}\right) + \sum_{s=\tau_1}^{\tau_2} \Phi\left(\frac{-1.5-m_s+10/24,t}{v_s+10/24,t}\right) \\
 &+ \sum_{s=\tau_1}^{\tau_2} \Phi\left(\frac{-0.5-m_s+7/24,t}{v_s+7/24,t}, \frac{-0.5-m_s+10/24,t}{v_s+10/24,t}, \rho_{s,t}\right) \\
 &- \sum_{s=\tau_1}^{\tau_2} \Phi\left(\frac{-3.5-m_s+7/24,t}{v_s+7/24,t}, \frac{-0.5-m_s+10/24,t}{v_s+10/24,t}, \rho_{s,t}\right) \\
 &- \sum_{s=\tau_1}^{\tau_2} \Phi\left(\frac{-0.5-m_s+7/24,t}{v_s+7/24,t}, \frac{-1.5-m_s+10/24,t}{v_s+10/24,t}, \rho_{s,t}\right) \\
 &+ 2 \sum_{s=\tau_1}^{\tau_2} \Phi\left(\frac{-3.5-m_s+7/24,t}{v_s+7/24,t}, \frac{-1.5-m_s+10/24,t}{v_s+10/24,t}, \rho_{s,t}\right).
 \end{aligned}$$

Here, $\Phi(\cdot)$ is st. nor. dist. f., while $\Phi(\cdot, \cdot, \rho)$ is the st. nor. dist. f. with correlation ρ .

Temperature Derivatives Pricing (Sec. 10.4): Application to Futures on Temperatures in Stockholm (Sec. 10.4.4)

They end their analysis of the weather markets with a discussion of futures contracts based on our fitted model for Stockholm data.

Their main emphasis is on the volatility term structure for the CAT and CDD futures. They investigate first the function

$$g(t) = e_1' \exp(At)e_p$$

which appeared in the volatility of Σ_{CDD} defined before:

Temperature Derivatives Pricing (Sec. 10.4): Application to Futures on Temperatures in Stockholm (Sec. 10.4.4)

$$dF_{CDD}(t, \tau_1, \tau_2) = \sigma(t) \int_{\tau_1}^{\tau_2} e_1' \exp(A(s-t)) e_p \times \Phi\left(\frac{m(t,s,e_1') \exp(A(s-t)) X(t)}{v(t,s)}\right) ds dB^\theta(t).$$

Inserting the estimates of the CAR(3) model for Stockholm data, we find that $g(t)$ is strictly positive for $t > 0$, which is illustrated in Fig. 10.20.

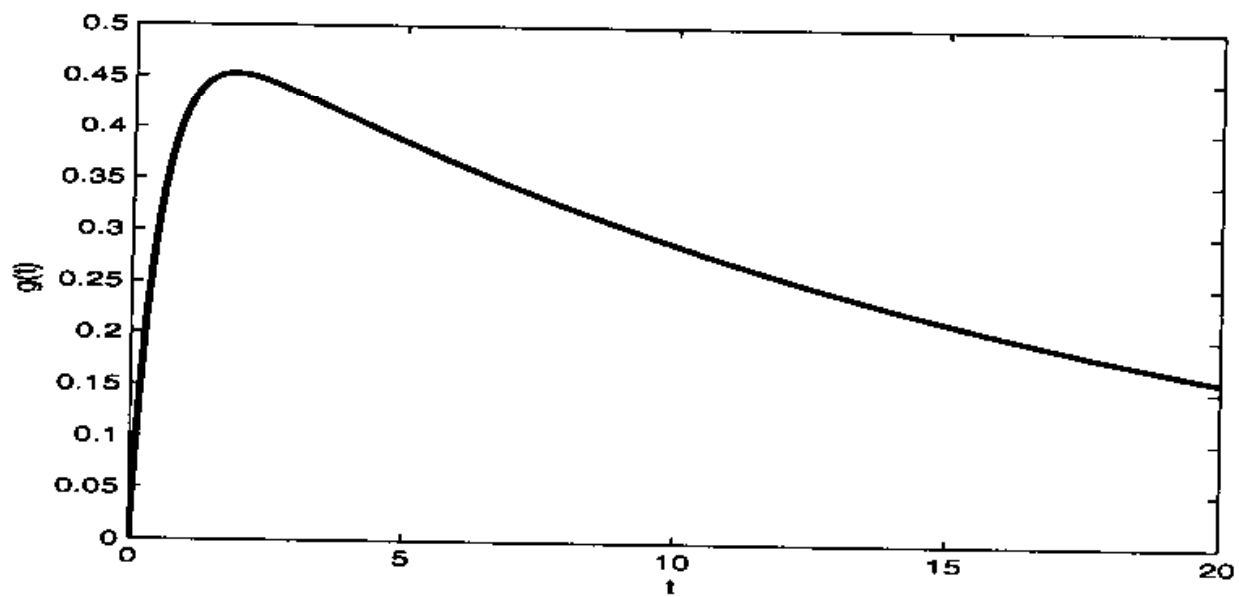


Fig. 10.20 The function $g(t)$ for the CAR(3) model for Stockholm data.

Function $g(t)$

Temperature Derivatives Pricing (Sec. 10.4): Application to Futures on Temperatures in Stockholm (Sec. 10.4.4)

Let us discuss how the CDD volatility looks like. Recall that it depends on $\mathbf{X}(t)$ and is thus stochastic. To understand the shape of volatility they suppose that $\mathbf{X}(t) = 0, T(t) = \Lambda(t), \theta = 0$. In Fig. 10.21 they plot the volatility for contracts with three different measurement periods.

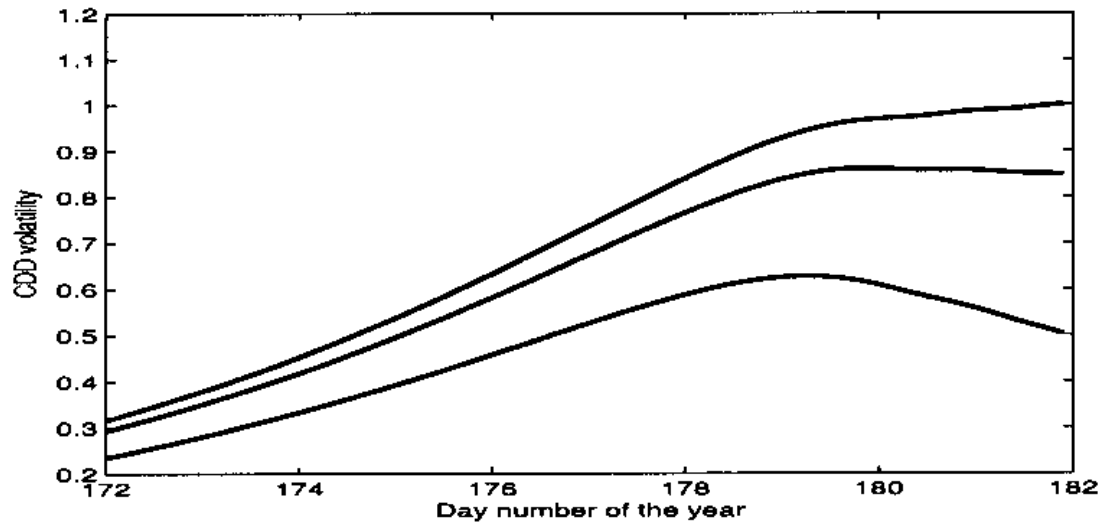


Fig. 10.21 The CDD volatility 10 days prior to start of measurement period, beginning 1 July (being day 182 of the year). The top graph shows the volatility of CDD measurement over the month of July, middle and the bottom graphs show the volatility for the first two weeks and the first week of July, respectively. The volatility is derived for the (unlikely) scenario that temperatures up to the beginning of the measurement period do not deviate from its seasonal mean $\Lambda(t)$.

Temperature Derivatives Pricing (Sec. 10.4): Application to Futures on Temperatures in Stockholm (Sec. 10.4.4)

In Fig. 10.22 they demonstrate the dynamics of the CDD volatility for two simulated temperature scenarios.

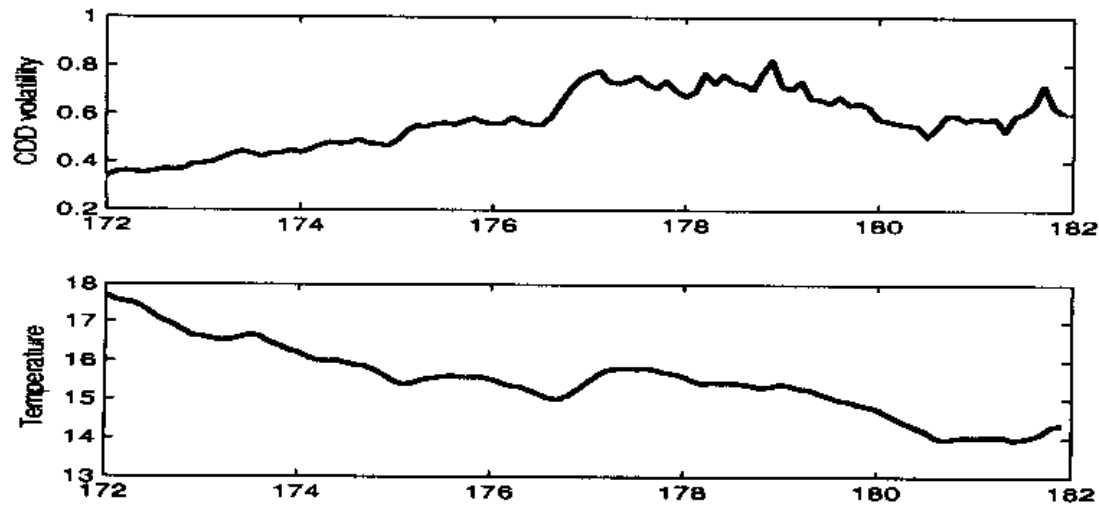


Fig. 10.22 The CDD volatility 10 days prior to start of measurement, beginning 1 July (day 182 of the year). The top graph shows the volatility for CDD measurement over the month of July. The bottom graph shows the simulated temperature for the same days.

Temperature Derivatives Pricing (Sec. 10.4): Application to Futures on Temperatures in Stockholm (Sec. 10.4.4)

They end with a graph showing the volatility for the CAT futures with the same measurement month of July (See. Fig. 10.23).

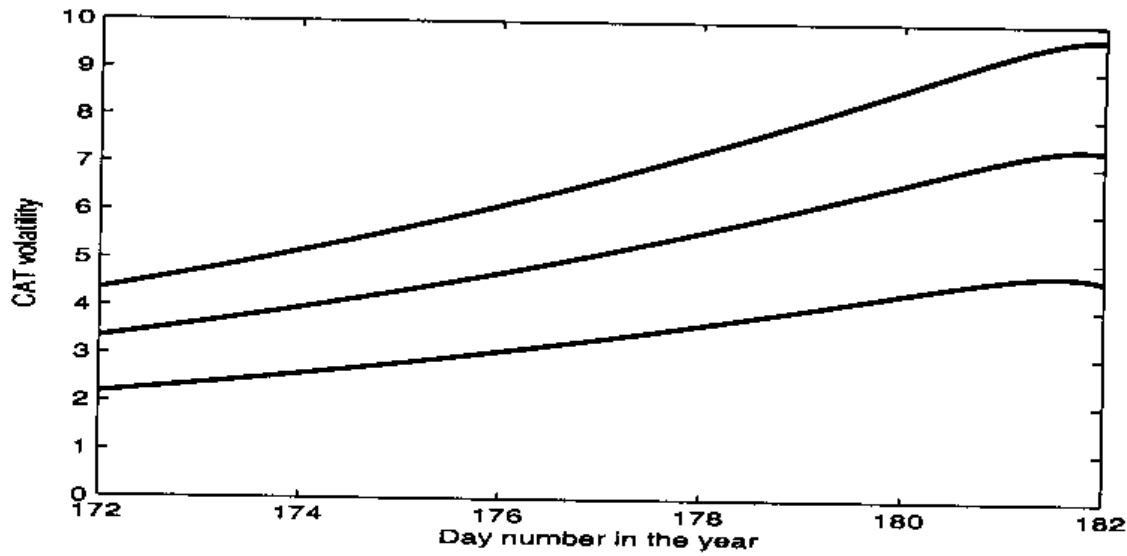


Fig. 10.23 The CAT volatility 10 days prior to start of measurement, beginning 1 July (day 182 of the year). The top graph shows the volatility of CAT measurement over the month of July, while the middle and the bottom show the volatility for the first two weeks and the first week of July, respectively.

Conclusion

1. Intro: Abstract
2. Some Preliminaries on Temperature Futures (sec. 10.1)
3. Modelling the Dynamics of Temperature (sec. 10.2)
4. Empirical Analysis of Stockholm Temperature Dynamics (sec. 10.3)
5. Temperature Derivatives Pricing (sec. 10.4)

This is the End of the Book! Congratulations!

Thank you very much for your patience, time and participation!